POLITECNICO DI TORINO
Repository ISTITUZIONALE

Mechanical and Thermal Behavior of Ultem® 9085 Fabricated by Fused-Deposition Modeling

Original
Mechanical and Thermal Behavior of Ultem® 9085 Fabricated by Fused-Deposition Modeling / Padovano, E., Galfione, M., Concialdi, P., Lucco, G., Badini, C.. - In: APPLIED SCIENCES. - ISSN 2076-3417. - ELETTRONICO. - 10:9(2020), p. 3170. [10.3390/app10093170]

Availability:
This version is available at: 11583/2829372 since: 2020-05-26T07:27:05Z

Publisher:
MDPI

Published
DOI:10.3390/app10093170

Terms of use:

This article is made available under terms and conditions as specified in the corresponding bibliographic description in the repository

Publisher copyright

(Article begins on next page)

14 September 2026

applied sciences

MDPI

Article

Mechanical and Thermal Behavior of Ultem® 9085 Fabricated by Fused-Deposition Modeling

Elisa Padovano [1,*], Marco Galfione [1], Paolo Concialdi [2], Gianni Lucco [2] and Claudio Badini [1]

[1] Politecnico di Torino, Department of Applied Science and Technology, Corso Duca degli Abruzzi 24, 10129 Torino, Italy; s253331@studenti.polito.it (M.G.); claudio.badini@polito.it (C.B.)
[2] Pininfarina S.p.A., Via Nazionale 30, 10020 Cambiano, Italy; p.concialdi@pininfarina.it (P.C.); g.lucco@pininfarina.it (G.L.)
* Correspondence: elisa.padovano@polito.it; Tel.: +39-0110904708

Received: 30 March 2020; Accepted: 28 April 2020; Published: 1 May 2020

Featured Application: Ultem 9085 is a relative new material with well-known flame-retardant properties that has many applications in digital manufacturing and rapid prototyping. Thanks to its high mechanical performance, this material has potential applications in many fields, especially aerospace, automotive, and military industries which require a high strength-to-weight ratio.

Abstract: Fused-deposition modeling (FDM) is an additive manufacturing technique which is widely used for the fabrication of polymeric end-use products in addition to the development of prototypes. Nowadays, there is an increasing interest in the scientific and industrial communities for new materials showing high performance, which can be used in a wide range of applications. Ultem 9085 is a thermoplastic material that can be processed by FDM; it recently emerged thanks to such good properties as excellent flame retardancy, low smoke generation, and good mechanical performance. A deep knowledge of this material is therefore necessary to confirm its potential use in different fields. The aim of this paper is the investigation of the mechanical and thermal properties of Ultem 9085. Tensile strength and three-point flexural tests were performed on samples with XY, XZ, and ZX building orientations. Moreover, the influence of different ageing treatments performed by varying the maximum reached temperature and relative humidity on the mechanical behavior of Ultem 9085 was then investigated. The thermal and thermo-oxidative behavior of this material was also determined through thermal-gravimetric analyses.

Keywords: fused-deposition modeling; mechanical properties; thermal behavior

1. Introduction

Additive manufacturing (AM) refers to an innovative technology used to fabricate three-dimensional components starting from a computer-aided design(CAD) model; this terminology was introduced by Charles Hull in 1986 and it was originally devoted to the production of prototypes. Recently, AM has attracted the growing interest of both scientific and industrial communities. In fact, thanks to its flexibility and ease of use, AM has progressively found its way into many manufacturing industries; in addition, it is one of the main topics of many researchers' studies. This innovative technology uses a conceptual approach which is completely different to that adopted by subtractive manufacturing methods, which start from a block of material and progressively remove part of this material through cutting, drilling, and grinding. These latter are typically used to create components for prototyping, manufacturing tooling, and end-use parts which require tight tolerances or geometries which are difficult to produce by molding, casting, or other traditional manufacturing techniques.

On the contrary, AM is based on an additive principle, which allows objects to be made starting from 3D-model data and using a layer-by-layer strategy to build up the desired part. There are many are the advantages connected with this technology, such as the possibility of manufacturing complex geometries, product customization and minimization of waste and scraps, in addition to a reduction in production costs as well as a simplification of the manufacturing cycle [1–3].

Fused-deposition modeling (FDM) was one of the first AM techniques introduced into the market for the production of polymeric components. It is defined as "a material extrusion process used to make thermoplastic parts through a heated extrusion and deposition of materials layer by layer" [4]. A continuous filament is heated at the nozzle, extruded, and then deposited to form stacked layers to build up the final component. The simplicity of the process and its low cost associated to its high speed are the main advantages of FDM. The main limitations of this technique are the anisotropic behavior of printed parts and their poor accuracy and surface finishing [5–7]; moreover, the formation of voids during the filament deposition is frequently observed [8–10]. This results in an increased porosity of final components and in a worsening of their mechanical properties. However, many studies have been performed in order to overcome these limitations.

Various materials are currently processed through FDM, such as acrylonitrile butadiene styrene (ABS), polylactide acid (PLA), polycarbonate (PC), polyamide (PA), polyphenylene sulphide (PPS); polyetherimide (PEI), and polyether ether ketone (PEEK) [11,12]. However, the development of new materials with customized properties represents a key challenge to further extend the potential large-scale application of FDM technology.

Ultem 9085 is a high-performance thermoplastic polymer manufactured by Stratasys which can be processed by FDM; it is a mixture of a polyetherimide (PEI) with a polycarbonate (PC) copolymer blend; the latter is added in order to improve the material flow [13].

It shows high glass transition temperature, excellent flame retardancy, low smoke generation, and good mechanical properties [14]. This set of properties makes this material a promising candidate in different application fields, especially those which require low mass and high strength such as aerospace, marine and automotive sectors. As Ultem 9085 is a relative recent material, no extensive literature is available. There are however, two main aspects that are more deeply investigated in the literature due to their large impact on the mechanical performance of printed parts. Firstly, the quality of final components is greatly influenced by the used-process parameters. FDM involves a quite complex mechanism based on the interaction of different parameters such air gap, raster width, raster angle, contour number, and contour width. Their optimization and the study of how these parameters can individually or collectively affect the properties of printed objects is fundamental to obtaining high performant components [15–18]. Secondly, mechanical properties are significantly affected by building orientation of samples; for this reason, some authors addressed their research toward this subject [13,19–21]. Other properties of Ultem 9085 have been only partially investigated. Cicala et al. [22] measured the rheological, morphological, and thermomechanical properties of Ultem 9085. In addition, Shelton et al. [23] focused their attention on the effect of the thermal profile of the FDM process on the inter-layer bonding of Ultem 9085 parts.

However, to the best of our knowledge, very limited literature is present on the study of thermal behavior of this material and on the effects that exposure to significant temperature and humidity variations may have on layer-by-layer 3D-manufactured parts. The promising performance of Ultem 9085 and its potential application in the transport sector, with particular reference to the automotive sector, generates interest in testing this material under severe environmental conditions.

Bagsik et al. [24] investigated the tensile properties of Ultem 9085 after long-term ageing which involved a conditioning time period up to 52 weeks and a subsequent exposure to specific temperature from −60 °C to 160 °C. These authors found that no change in geometry occurred after a long period of storage in different environmental conditions; on the contrary, the strength properties worsened when increasing test temperatures were applied.

The present paper investigates the mechanical properties of Ultem 9085 as a function of building directions. The influence on the mechanical behavior of different ageing treatments, performed by varying the environmental conditions in terms of maximum-reached temperature and relative humidity, were also studied. In addition, the thermal and thermo-oxidative behavior of this material was investigated.

2. Materials and Methods

This work focused on Ultem 9085, a high-performance thermoplastic polymer specifically designed for FDM technology; it is supplied by Stratasys in the form of natural-colour filament with a diameter of 1.75 mm. This material was used for the preparation of specimens by using a Fortus 450mc 3D-printer supplied by Stratasys. The fabrication of samples consists of three main steps. Firstly, the test coupons were modelled using the commercial software Solidworks, and then a machine code in STL (stereolithography) format was generated. Secondly, the STL file was exported into the software package Insight 12.1, which was supplied with the AM machine. It was used to set the build parameters and control all the printing stages. All the samples were fabricated by using the same building parameters: raster width of 0.508 mm, contour width of 0.508 mm, air gap of 0 mm, and contour number of 3. Moreover, filling of layers (a theoretical 100% infill was set) was performed alternating raster angles of ±45° with respect to the x-axis. Finally, the STL file was sent to FDM machine, which began to fabricate the specimens by extruding Ultem 9085 filament and depositing it layer by layer. The scanning strategy involved the deposition of the contour of a single layer followed by its filling according to the prefixed raster angle. A nozzle with a T16 tip compatible with Stratasys's equipment and showing a diameter of 0.4064 mm was used. For all other process parameters, fixed default settings supplied by Stratasys and saved in the management software were used [25].

The specimens for tensile and bending tests were manufactured according to XY, XZ, and ZX building orientations (Figure 1), where the first letter specifies the direction of the main axis of the specimen with respect to the build platform, and the second letter, together to the first one, identifies the plane on which the largest sample surface lies.

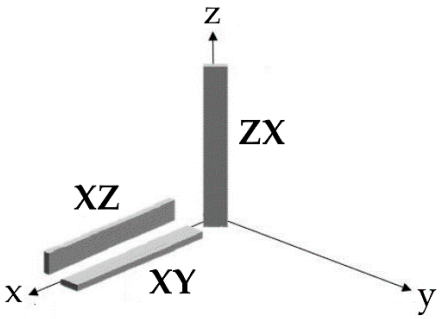

Figure 1. FDM samples built according XY, XZ, and ZX directions.

The density of both filament and printed components (with size $10 \times 10 \times 10$ mm^3) was measured by Archimedes' method using methanol as the immersion medium—the volume of displaced liquid corresponded to the samples' volume. The mass of both filament and samples was weighed by using a balance with an accuracy of 1.0×10^{-5} g. The measurements were repeated on sets of five samples for each building orientation; average values and their standard deviations were calculated.

Mechanical tests were performed using a universal testing machine (MTS Criterion Model 43, MTS Systems s.r.l., Italy) equipped with a 5 kN load cell; the configuration of the equipment was adapted to the different kinds of mechanical test. ASTM D638-14 was used as reference for the fabrication of samples and the measurement of yield strength, ultimate tensile strength, elastic modulus, and elongation at break of Ultem 9085 specimens. The average values of each property and the relevant standard deviations were calculated. Type I dog-bone samples were built according the following

dimensions—overall length of 165 mm, thickness of 3.2 mm, and length and width of narrow section of 57 mm and 13 mm, respectively. The tensile tests were carried out on 15 samples (5 for each building direction) setting a strain rate of 5 mm/min in accordance to the previously-mentioned test standard; a 25 mm gauge-length extensometer was used for strain measurements.

Fracture surfaces of samples with different building orientations were observed by using Leica MS5 stereo microscope, Leica, Heidelberg equipped with Leica LAS software.

Three-point flexural tests were performed on a set of 15 specimens (5 for each building orientation) following the ASTM D790-17 standard. The results were averaged, and the standard deviation values were calculated. Rectangular bars with a length of 127 mm, a width of 12.7 mm, and 3.2 mm high were built; all the specimens were maintained at a fixed temperature of 87 °C for 12 h before performing the mechanical tests. The tests determined the flexural strength, the elastic modulus, and flexural strain of samples. A test specimen with rectangular cross section was placed in a flat position on two supports; the span length between them was fixed to 51.2 mm in accordance with the test standard. The load was then applied by means of a loading nose located in the centre of the span length; a crosshead rate of 1 mm/min was used. The specimen was deflected until rupture occurred or until a maximum strain of 9.0% was reached.

For both tensile and flexural properties average values and standard deviations were calculated. All data were statistically evaluated using one-way ANOVA. Post hoc Tukey's honestly significant difference(HSD) multiple comparison tests were then used to identify statistically-homogeneous subsets ($\alpha = 0.05$).

The thermal stability of Ultem 9085 (in the form of filament and printed samples) was evaluated through thermal-gravimetric analyses (TGA/SDTA851 Mettler Toledo), which were carried out from 25 to 800 °C with a heating rate of 10 °C/min under both argon atmosphere and air (gas flowing at 50 mL/min). The presence of any crystalline phases in the solid residue obtained after the thermal degradation of Ultem 9085 in inert atmosphere was investigated by using X-ray diffraction (Panalytical X'PERT PRO PW3040/60, Cu Kα radiation at 40 kV and 40 mA, Panalytical BV, Almelo, The Netherlands). The spectrum was collected in 2 Theta range from 10° to 80° setting a step size of 0.013°.

The ageing behavior of Ultem 9085 was evaluated after three kinds of artificial ageing treatments:

- Warm storage, which consisted of maintaining samples at a temperature of 100 °C and a zero percent relative humidity for a period of 7 days;
- Cyclic climate change, involving the constant and periodic variation of climate cell temperature between −40 and +90 °C using a thermal gradient of 1 °C/min. Both the maximum and minimum temperatures were maintained for 4 h; the relative humidity was also controlled reaching a maximum of 85% at 90 °C. This cycle was repeated for 10 times with a cumulative duration of 120 h;
- Thermal shock, consisting of two steps. Firstly, the samples were maintained at the temperature of 70 °C and zero relative humidity for 7 days. They then were subjected to a strong temperature variation up to −20 °C for 24 h.

To the best of authors' knowledge, there is not a standard procedure to determine the thermal behavior of a car component in different environmental conditions. However, some studies in the literature investigated the vehicle cabin temperatures that can be reached in various weather conditions and during the different periods of the year [26–28]. The testing conditions adopted for the three previously-described ageing treatments aim to simulate the environmental conditions (in term of temperature and relative humidity variations) that an internal vehicle component experiences during its life cycle. They are currently used for the qualification and validation of internal components in automotive industry.

Bars for flexural tests were subjected to the three kinds of previously-described environmental tests—sets of four samples were subjected to a single ageing treatment and a fourth one underwent all the treatments. The influence of the ageing treatments on the mechanical behavior of Ultem 9085 was

investigated by carrying out flexural tests to samples which underwent a single ageing cycle (samples set A, after warm storage; samples set B, after cyclic climate change; and samples set C, after thermal shock) or all the three treatments (samples set D). A total of 16 specimens with building orientation XZ (which previously showed the best mechanical performance) were tested following the guidelines of ASTM D790-17 standard. The average values of flexural strength, elastic modulus, and elongation at break and their standard deviations were reported. The obtained results were statistically evaluated using one-way ANOVA. Moreover, post hoc Tukey's HSD tests were performed in order to identify the environmental conditions that significantly affected the flexural performances of Ultem 9085 ($\alpha = 0.05$).

3. Results and Discussion

3.1. Density

The measurement of density was performed on the Ultem 9085 in the form of both filament and printed components. The results are reported in Table 1.

The density of the filament was found to be equal to 1.2864 ± 0.0005 g/cm^3; this value was taken as reference to calculate the relative density of printed samples as well as the porosity values.

Table 1. Average values of densities and porosity (standard deviations in parenthesis) of printed parts for the different building orientations.

Building Orientation	Density (g/cm^3)	Relative Density (% of Theoretical)	Porosity (%)
XY	1.2389 (0.0004)	96.40 (0.03)	3.60 (0.03)
XZ	1.2552 (0.0003)	97.30 (0.02)	2.69 (0.02)
ZX	1.2637 (0.0002)	97.96 (0.02)	2.04 (0.02)

From Table 1 it is evident that samples showed increasing relative density in the printing directions XY < XZ < ZX; as expected, the corresponding values of calculated porosity showed a reverse trend. This trend of density variation when different printing directions are considered agrees with that observed by Byberg et al. [25]. However, these authors reported values of density in the range from 89.6% to 92.1%, therefore quite a lot lower than those presently obtained.

The variation of density observed for the different building orientations is mainly influenced by the ratio between the extent of the contour and the infill zones, and the scanning strategy adopted to fill each layer. The extruder head firstly deposits the contour of the object outlining its perimeter; then, it completes the layer by depositing the filament within the layer contour with an orientation of +45°/−45°. The misalignment of the infill with respect to the contour causes the formation of voids—in fact, when the +45°/−45° filament meets the contour and goes back towards the opposite side, an empty space is left at the corner of infill filament. The higher the infill area involved in the formation of each layer, the higher the fraction of formed voids.

3.2. Mechanical Properties

3.2.1. Tensile Tests

Tensile tests were performed on dog-bone specimens with building orientation XY, XZ, and ZX, respectively.

The statistical experiment was carried out using the one-way analysis of variance (ANOVA) in order to evaluate the main effects of building orientations (the independent variables) on each tensile property under investigation (yield strength, ultimate tensile strength, elastic modulus, and elongation at break, which are the response variables). Specifically, the *p*-value which indicates the level of significance of the different factors within a statistical test is reported; it represents the probability

of a factor affecting the mechanical properties. The significant factors are tested with p-value lower than 0.05.

The statistical analysis (Table 2) revealed significant differences among building orientations for all the tensile properties under investigation; this implies that at least one of them differs from the others. The Tukey's HSD post hoc test ($\alpha = 0.05$) was performed in order to identify which pairs of building directions are significantly different from each other.

Table 2. ANOVA tests for tensile properties.

Mechanical Property	Source	Sum of Squares	F	F Crit	p-Value
Yield strength	BG WG	131.961 10.722	750.954	3.885	<0.001
Ultimate tensile strength	BG WG	131.961 10.722	120.109	3.885	<0.001
Elastic modulus	BG WG	74,080 105,680	4.206	3.885	0,040
Elongation at break	BG WG	109.256 6.856	95.608	3.885	<0.001

BG = between groups; WG = within groups; SS = sum of squares; F = F ratio; F crit = critical F ratio.

Table 3 shows the means and the standard deviations for the tensile properties such as yield and ultimate tensile strengths, elastic modulus, and elongation at break; moreover, it compares these outcomes with those present in the technical datasheet provided by Stratasys (in this case, specimens were built by using Fortus 3D printer setting default process parameters defined by Stratasys).

Table 3. Results of tensile properties of Ultem 9085 samples built according the three building directions XY, XZ, and ZX, mean values, and standard deviations (in parentheses). Superscript letters indicate statistically-homogeneous subsets (Tukey's HSD test, $\alpha = 0{:}05$).

Mechanical Property	XY	XZ		ZX	
	Experimental	Experimental	Datasheet	Experimental	Datasheet
Yield strength [MPa]	47.0 (0.6) ^{b}	54.8 (0.3) ^{c}	47	32.0 (1.5) ^{a}	33
UTS [MPa]	65.9 (0.7) ^{b}	73.0 (1.3) ^{b}	69	39.6 (6.0) ^{a}	42
Tensile modulus [MPa]	2220 (54) ^{a}	2300 (54) ^{a}	2150	2128 (144) ^{a}	2270
Elongation at break [%]	6.6 (0.6) ^{b}	8.0 (0.2) ^{b}	5.8	1.7 (0.8) ^{a}	2.2

It is evident that XZ orientation was the most performant one showing the highest values of yield and ultimate tensile strengths (UTS), elastic modulus, and elongation at break. However, pairwise multiple comparisons with Tukey's HSD test revealed that UTS, tensile modulus, and elongation at break of XY samples were not significantly different with respect to those determined for XZ specimens. On the other hand, ZX samples reported statistically lower tensile properties compared to the both XY and XZ building directions. Despite the value of tensile modulus for ZX samples not being significantly different from those obtained for the other two orientations, tensile strength and elongation at break were much lower with respect to those observed for XY and XZ directions. The observed trend for tensile properties is in good agreement to that reported in the literature [10,13,20,25].

A comparison between the experimental results and the mechanical properties reported in the technical datasheet (Table 3) is possible only for the best and worse performant building directions, XZ and ZX, respectively. For XZ orientation, all the measured mechanical properties were slightly higher than those stated by the manufacturer; on the contrary, this was not observed for samples printed in the ZX direction. In this case in fact, the measured properties were slightly lower than those reported in the material datasheet. Moreover, the standard deviation associated to the tensile properties of ZX

samples was higher with respect to those calculated for XY and XZ samples; this implies a higher dispersion of the data.

Samples after tensile tests are shown in Figure 2a–c. These images provide evidence of the different filament deposition patterns adopted for the building of samples with XY, XZ, and ZX orientations, respectively. Figure 2d–f show the fracture surfaces of the three kinds of samples. From a visual analysis it seems that ZX cross section shows lower porosity degree than XY and XZ samples. The presence of few voids can in fact be observed mainly in the region close to the interface between infill and contour (red arrows). Similarly, in XZ samples the porosities seem mainly located at the border area where infill and contour filament meet; however, the amount of observed voids seems higher than for ZX samples. Moreover, the visual inspection of XY surface fracture evidences the presence of some voids both at the interface infill/contour and in the infill area. These qualitative observations agree to the density values reported in Table 1.

The comparison of fracture surfaces evidences some differences in the fracture behavior of samples as a function of the different building orientations.

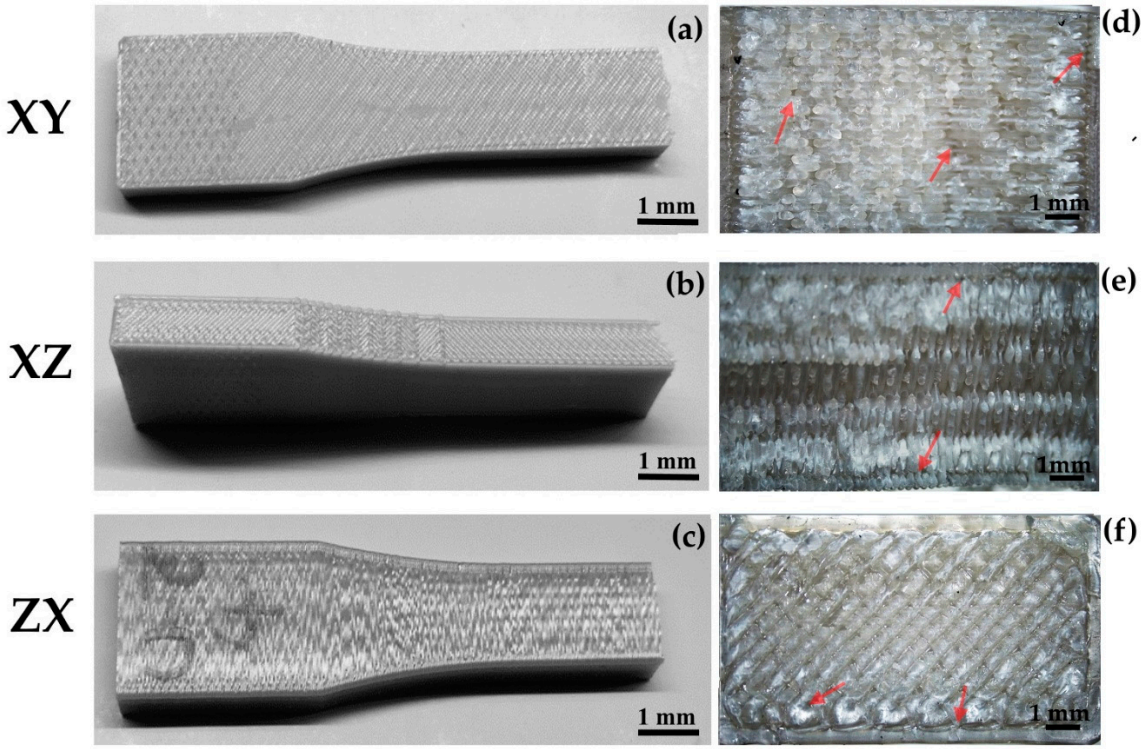

Figure 2. Samples built in XY, XZ, and ZX building directions after tensile tests. Macroscopic views of samples (**a**–**c**) and fracture surfaces (**d**–**f**).

Both XY and XZ specimens, which granted the best tensile properties, showed a brittle fracture. The slightly higher UTS of XZ samples with respect to the XY ones was probably due to the different contour/infill areas ratio. The observed fracture surfaces show a rectangular shape where most of the area is constituted by the infill, and only a minority part represents the contour. In both XY and XZ samples, the filament which forms the contours is deposited parallel to sample axes and, as a consequence, in the same direction of load application. This allows filaments to strongly oppose to the load application. On the other hand, the filaments which constitute the infill are placed at 45° with respect to the direction of load application. In samples with XZ orientation, the contour/infill areas ratio is higher with respect to XY samples because of the contour is present on the longest side of the rectangular cross section (while in the XY samples, the contour represents the shortest side). This may explain both the higher strength and elongation of XZ specimens with respect to XY ones.

In addition, the improved mechanical behavior of XZ samples with respect to XY ones can be supported by the higher degree of porosity observed in XY samples with respect to XZ ones; the porosity can in fact negatively affect the mechanical properties of the material.

The fracture surface of ZX samples is quite different from those previously discussed; it is quite flat, and the disposition of filaments at 45 °C can be clearly seen. This suggests that the fracture mechanism involves the debonding among layers, whose adhesion cannot withstand too high tensile loads. The fracture mechanism proposed for ZX samples fabricated by fused-deposition modeling was formerly reported in the literature [20,29]. The debonding at the interfaces placed perpendicular to the tensile load are also responsible for the lower strength and elongation at break.

The very good compromise between strength and ductility experimentally observed justifies the growing interest of scientific and industrial communities for Ultem 9085 material. It is worth highlighting that this material shows an ultimate tensile strength comparable to that of PA12 reinforced with carbon fibres (UTS = 76 MPa) provided by the same manufacturer [30].

3.2.2. Flexural Tests

The three-point bending tests were performed according to ASTM D790-17 standard; the statistical analysis of flexural strength and modulus results is reported in Table 4.

Table 4. ANOVA test for flexural strength and modulus.

Mechanical Property	Source	Sum of Squares	F Ratio	*p*-Value
Flexural strength	BG WG	3422.889 4.460	767.521	<0.001
Elastic modulus	BG WG	295,285.267 1416.533	208.456	<0.001

As previously observed for tensile properties, the *p*-values indicate that there is was a significant difference among building orientations for the flexural properties under investigation. The Tukey's HSD post hoc test was performed with the aim of identifying which building direction was significantly different from the others. Table 5 reports the values of flexural strength, elastic modulus, and flexural strain in term of means and standard deviations for each building direction.

Table 5. Flexural properties of Ultem 9085 with XY, XZ, and ZX orientations, means, and standard deviations (in parentheses). Superscript letters indicate statistically homogeneous subsets (Tukey's HSD test, $\alpha = 0.05$).

	XY	XZ		ZX	
	Experimental	Experimental	Datasheet	Experimental	Datasheet
Flexural strength [MPa]	109.72 (0.81) ^{b}	117.98 (0.26) ^{c}	112	69.98 (3.67) ^{a}	68
Flexural modulus [MPa]	2315 (58) ^{b}	2428 (17) ^{c}	2300	1963 (27) ^{a}	2050
Strain at break [%]	No break	No break	No break	3.6 (0.2)	3.7

These results confirm that samples with XZ orientation showed the best mechanical performances; in fact, the Tukey's HSD test revealed the significantly highest flexural strength and modulus for XZ samples compared to the other building directions. These values of flexural properties are slightly higher with respect to those reported in the material datasheet (these latter refer to samples built by using Fortus 3D printer setting default process parameters defined by Stratasys), as previously observed for tensile properties.

Specimens with XY orientation had significantly lower flexural properties than XZ samples. This is in good agreement with the results obtained by Byberg et al. [25] on samples printed using similar process parameters.

Moreover, according to Motaparti et al. [17] the better flexural strength of XZ coupons with respect to XY ones can be attributed to the different arrangement of contour in samples with different building orientation. When a flexural load is applied, the top surface of the specimen experiences compression, while the bottom one is under tension. In the case of XZ specimens both the top and bottom surfaces, where the stress is maximum, are mainly constituted by the contour. The presence of filaments perpendicular to the load application allow higher resistance value to be obtained. On the contrary, in XY samples the two load-bearing surfaces are mainly constituted by the infill, while the contour is only a small fraction located in the external part of the surface. This decreases the maximum load that the samples can withstand.

A significant worsening of flexural behavior was observed for ZX samples. Their flexural strength and modulus were about 40% and 20% lower than the values observed for XZ samples. Moreover, XY and XZ samples plastically deformed until the maximum value of strain was reached. On the contrary, the same tests performed on ZX samples led to the premature failure of samples at low value of strain; this provided evidence of their brittle behavior. The arrangement of interfaces among stacked layers, which are perpendicular with respect to the sample axis, and therefore parallel to the load application can be considered the main cause of the different flexural and deformation features of ZX samples.

The experimental results conclusively showed that the building direction has a significant effect on both the tensile and flexural properties. Samples with XZ orientation showed the best performances, while slightly lower mechanical properties were observed for XY specimens. On the contrary, the arrangement of stacked layers in ZX samples represents the main weakness of these samples when they are subjected to both tensile and flexural loads.

3.3. Thermal Behavior

Thanks to its good mechanical performances, Ultem 9085 material has many potential applications in the aerospace, automotive, and military industries. However, good mechanical properties are not the only requirements that a material has to satisfy for these kinds of applications. Although this material is known as flame retardant showing low smoke emission and low smoke toxicity [14], its thermal stability at high temperature and under different environmental conditions have been scarcely investigated.

3.3.1. Thermal-Gravimetric Analyses

Thermal-gravimetric analyses (TGA) were performed on the starting filament and the printed samples in order to investigate their thermal stability in a temperature range from 25 °C to 800 °C. However, no differences were observed between TGA curves of the filament and the specimens when they were independently tested in the air and argon atmospheres. This suggests that the FDM process did not influence the material thermal and thermo-oxidative degradation processes.

Figure 3 compares the TGA and derivative-TGA curves for Ultem 9085 under oxidizing (Figure 3a) and inert (Figure 3b) atmospheres.

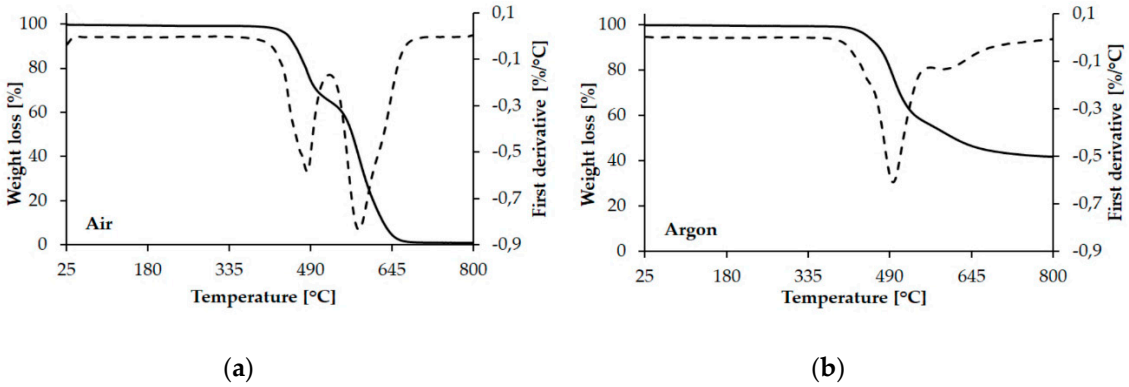

(**a**) (**b**)

Figure 3. TGA (continuous lines) and D-TGA (dotted lines) curves for Ultem 9085 under (**a**) air and (**b**) argon atmosphere.

Both the curves collected in air and argon atmospheres show an initial degradation temperature (conventionally, it corresponds to the temperature at which there is a weight loss equals to 5%) of about 447.5 °C.

However, a significant difference in terms of solid residue could be observed—the thermo-oxidative degradation of Ultem 9085 was almost complete in air, leaving a residue of about 1%; on the contrary, a residue of about 44% with respect to the initial weight was observed after heating the material in inert atmosphere up to 800 °C. These results are comparable to those obtained by Lisa et al. [31] who investigated the thermal and thermo-oxidative stability of some polyetherimide; these authors reported a lower residue quantity when heating PEI in air (14–22 wt% at maximum temperature of 700 °C) with respect to inert atmosphere (43–54 wt%).

XRD analysis was performed on the solid residue obtained after degradation in inert atmosphere to investigate its composition. The XRD spectrum (Figure 4) shows the presence of a broad hump in 2theta range from 15° to 30° only; additional crystalline phases were not observed. This implies that the residual fraction is mainly constituted by amorphous carbonaceous species.

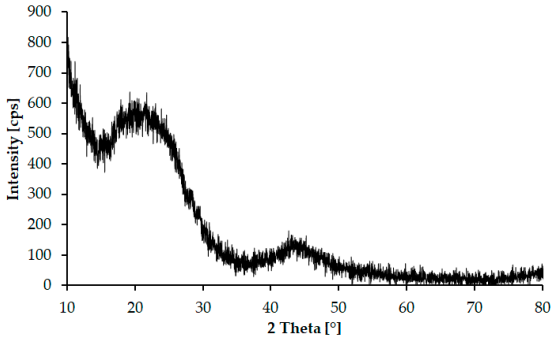

Figure 4. XRD pattern of Ultem 9085 solid residue obtained after thermal degradation.

The degradation of the material under investigation always occurred in two steps; the D-TGA curves show two peaks which correspond to the maximum rates of weight loss detected at 484.2 °C and 582.5 °C in air and at 495.8 °C and 592.5 °C in argon, respectively. The two-step degradation mechanism can be explained considering that Ultem 9085 is a mixture of PEI and polycarbonate (PC) copolymer blend; the latter is added in order to improve the material flow [13].

According to Feng et al. [32] the degradation of polycarbonate in inert atmosphere shows only one degradation step; the maximum degradation temperature is observed at 504.8 °C. On the basis of this outcome, the first degradation step of Ultem 9085 can be attributed to PC, and the second one to the degradation of PEI. A comparison between the intensity of the peak at higher temperature in

D-TGA curves is evidence of a different degradation mechanism of PEI component in air as compared to argon atmosphere.

3.3.2. Ageing Tests

The thermal behavior of Ultem 9085 was evaluated after different artificial ageing treatments:

- Warm storage, which had the aim of verifying the maintenance of high mechanical properties of the components after a long period at high temperature;
- Cyclic climate change, which allowed evaluation of the stability of the material under investigation under a constant and periodic variation of both the temperature and humidity. These variations could in fact cause reactions of hydrolytic degradation or cracks due to water penetration and freezing;
- Thermal shock, which aimed to verify the resistance of Ultem 9085 to sudden temperature variations.

In order to evaluate the effect of different ageing treatments on mechanical behavior of Ultem 9085, three-point flexural tests were performed on samples with XZ orientation (they showed the highest flexural properties, as reported in Table 5) after each ageing step (sets A, B, and C in Table 6). A set of samples was tested after the three ageing treatments (set D in Table 6).

Table 6. Tested samples after different ageing treatments.

Ageing Treatment	Set of Tested Samples	
Warm storage	A	D (A + B + C)
Cyclic climate change	B	
Thermal shock	C	

Figure 5 compares the average stress–strain curve of as-printed samples with those of specimens after different ageing treatments.

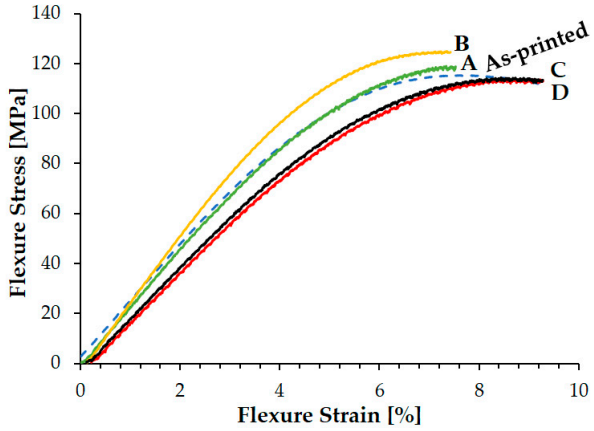

Figure 5. Stress–strain curves of samples after different ageing treatments.

The statistical analysis was performed by considering the flexural properties of Ultem 9085 samples before and after ageing treatments. The results of one-way ANOVA (Table 7) showed that the ageing factor had a significant effect on the average values of flexural strength and elastic modulus. Therefore, the Tukey's HSD post hoc test was performed with the aim of identifying which environmental conditions are significantly different from the others, mainly affecting the mechanical performances of the material.

The results in term of flexural strength, elastic modulus, and elongation at failure are reported in Table 8; these outcomes are compared to the mechanical properties of as-processed samples.

The maintenance of samples at high temperature (100 °C) for a long period in a dry environment (Figure 5, curve A) did not involve a significant variation of flexural properties with respect to those observed for as-printed specimens (Table 5). However, differently from these latter samples, samples A showed break at an elongation value close to the maximum that can be reached (as previously reported, the load was applied until the breakage of samples occurred or until a maximum strain of 9% was reached).

Table 7. ANOVA test for flexural strength and modulus obtained after ageing treatments.

Mechanical Property	Source	Sum of Squares	F Ratio	*p*-Value
Flexural strength	BG WG	785.737 803.0275	3.914	0.021
Elastic modulus	BG WG	1,346,911 316,574.2	17.018	<0.001

Table 8. Mechanical properties of Ultem 9085 after different ageing treatment. Superscript letters indicate statistically homogeneous subsets (Tukey's HSD test, $\alpha = 0.05$).

Mechanical Property	A	B	C	D	As Printed
Flexural strength [MPa]	118.8 (7.7) ^{a,b,c}	124.7 (5.3) ^{c}	113.4 (1.7) ^{a}	113.7 (13.3) ^{a,b,c}	118.0 (0.3) ^{b}
Elastic modulus [MPa]	2201(227) ^{b}	2650 (199) ^{c}	2030 (75) ^{a}	1956(93) ^{a}	2428 (17) ^{b}
Elongation at break [%]	7.5 (0.1)	7.5 (0.1)	No break	No break	No break

On the contrary, a significant variation of mechanical properties can be observed for samples C: the stay at the temperature of 70 °C for a long time followed by a sudden temperature variation up to −20 °C (Figure 5, curve C) leading to a significant decreasing of elastic modulus and flexural strength with respect to the as-printed samples.

Specimens that withstood cyclic climate change (Figure 5, curve B) also experienced a significant variation of temperature (the difference between minimum- and maximum-reached temperatures was 90 °C) accompanied by a change of relative humidity. The so-conditioned specimens showed a significant improvement of elastic modulus and flexural strength with respect to as-printed and aged samples. The material with increased stiffness broke at a strain value of 7.5%.

These outcomes suggest that an important thermal variation, independently from the thermal gradient, has a significant effect on Ultem 9085.

The results of Tukey's HSD post hoc test did not show a significant difference in term of elastic modulus for samples which underwent warm storage, cyclic climate change, thermal shock (Figure 5, curve D), and thermal shock only (Figure 5, curve C). This confirms that an important temperature variation has the greatest effect on mechanical behavior of the material under investigation. Moreover, it is worth nothing that the flexural strength after the three considered treatments was not significantly different from that of as printed material. Therefore, the mechanical performances of Ultem 9085 can still be considered good after the different ageing treatments. This confirms the reliability of Ultem 9085 after ageing treatments at different temperature and humidity conditions.

4. Conclusions

Fused-deposition modelling was used to process Ultem 9085, a thermoplastic polymer which has recently attracted the interest of scientific and industrial communities thanks to its good properties such as excellent flame retardancy, low smoke generation, and high mechanical performances.

In order to acquire a deeper knowledge of Ultem 9085, which is a promising candidate in many application fields, it was characterized in term of mechanical and thermal properties.

Tensile and flexural tests were performed on samples with XY, XZ, and ZX building directions. XZ orientation showed the highest yield and ultimate tensile strengths, elastic modulus, and elongation at break; however, these properties were found not to be significantly different for samples with XY

orientation (with the exception of elastic modulus which was similar for the two kind of samples). On the contrary, ZX samples reported significantly lower tensile properties; this is due to the fact that the fracture of these samples is caused by debonding among layers, whose adhesion cannot withstand too high tensile loads. A similar trend was observed for flexural properties—XZ samples in fact showed the highest strength and modulus; however, these properties were significantly lower for both XY and ZX samples.

These outcomes confirm the excellent mechanical properties of Ultem 9085 built according XZ orientation, and provide evidence that that the building direction has a significant effect on tensile and flexural properties.

The effect of ageing treatments performed by varying the environmental conditions in term of maximum reached temperature and relative humidity on the flexural behavior of samples with XZ orientation (the most performance one) was also investigated.

Warm storage, which involves the maintenance of samples at 100 °C and zero relative humidity for a long period, did not show a significant impact on mechanical properties of Ultem 9085.

On the contrary, a sudden variation of temperature from 70 °C to −20 °C negatively affected the properties of the material under investigation, which showed a significant decreasing of both flexural strength and elastic modulus with respect to the as-printed samples. When the temperature variation was gradual, as with that experienced by Ultem 9085 during cyclic climate change, a significant improvement of flexural strength and modulus was observed.

Ultem 9085 was conclusively found to be sensitive to a sudden variation of the temperature; however, maintenance of high temperature, or a progressive variation of temperature, did not seem to significantly affect the very good mechanical performances of this material.

The thermal and thermo-oxidative behavior of this material was investigated and it was found to show no significant weight variation up to the temperature of 447.5 °C. The degradation mechanism involves two steps, which correspond to degradation of PC and PEI components, respectively.

Author Contributions: Conceptualization, G.L. and C.B.; methodology, P.C. and E.P.; software, M.G.; validation, M.G. and E.P.; investigation, M.G.; resources, E.P. and P.C.; data curation, M.G. and E.P.; writing—original draft preparation, E.P.; writing—review and editing, E.P., M.G., and C.B.; visualization, E.P.; supervision, C.B., P.C., and G.L.; project administration, G.L. and C.B. All authors have read and agreed to the published version of the manuscript.

Funding: This research received no external funding.

Acknowledgments: The authors gratefully acknowledge the technical support provided by Raffaella Grandi, Strategic Account Manager at Stratasys and Dott. Giacomo Cacciani, Head of Additive Manufacturing Division at Overmach. The authors also thank Mario Pietroluongo who provided insight and expertise that assisted the research activities.

Conflicts of Interest: The authors declare no conflict of interest.

References

1. Boschetto, A.; Bottini, L. Robotics and Computer-Integrated Manufacturing Design for manufacturing of surfaces to improve accuracy in Fused Deposition Modeling. *Robot. Comput. Integr. Manuf.* **2016**, *37*, 103–114. [CrossRef]
2. Yang, S.; Tang, Y.; Zhao, Y.F. A new part consolidation method to embrace the design freedom of additive manufacturing. *J. Manuf. Process.* **2015**, *20*, 444–449. [CrossRef]
3. Baumers, M.; Dickens, P.; Tuck, C.; Hague, R. Technological Forecasting & Social Change The cost of additive manufacturing: Machine productivity, economies of scale and technology-push. *Technol. Forecast. Soc. Chang.* **2016**, *102*, 193–201.
4. International, A. *ASTM F2792-12a Standard Terminology for Additive Manufacturing Technologies*; ASTM International: West Conshohocken, PA, USA, 2020.
5. Equbal, A.; Islamia, J.M.; Sood, A.K.; Technology, F. Optimization of process parameters of FDM part for minimiizing its dimensional inaccuracy. *Int. J. Mech. Prod. Eng. Res. Dev.* **2017**, *7*, 57–66.

6. Boschetto, A.; Bottini, L.; Veniali, F. Integration of FDM surface quality modeling with process design. *Addit. Manuf.* **2016**, *12*, 334–344. [CrossRef]
7. Ngo, T.D.; Kashani, A.; Imbalzano, G.; Nguyen, K.T.Q.; Hui, D. Additive manufacturing (3D printing): A review of materials, methods, applications and challenges. *Compos. Part B* **2018**, *143*, 172–196. [CrossRef]
8. Wang, X.; Zhao, L.; Ying, J.; Fuh, H. Effect of Porosity on Mechanical Properties of 3D Printed Polymers: Experiments and Micromechanical Modeling Based on X-ray Computed Tomography Analysis. *Polymers* **2019**, *11*, 1154. [CrossRef]
9. Kulkarni, P.; Dutta, D. Deposition Strategies and Resulting Part Stiffnesses in Fused Deposition Modeling. *J. Manuf. Sci. Eng.* **1999**, *121*, 93–103. [CrossRef]
10. Zaldivar, R.J.; Mclouth, T.D.; Ferrelli, G.L.; Patel, D.N.; Hopkins, A.R.; Witkin, D. Effect of initial fi lament moisture content on the microstructure and mechanical performance of ULTEM® 9085 3D printed parts. *Addit. Manuf.* **2018**, *24*, 457–466. [CrossRef]
11. Jiang, S.; Liao, G.; Xu, D. Mechanical properties analysis of polyetherimide parts fabricated by fused Mechanical properties analysis of polyetherimide parts fabricated by fused deposition modeling. *High Perform. Polym.* **2018**, *31*, 97–106. [CrossRef]
12. Geng, P.; Zhao, J.; Wu, W.; Ye, W.; Wang, Y.; Wang, S.; Zhang, S. Effects of extrusion speed and printing speed on the 3D printing stability of extruded PEEK filament. *J. Manuf. Process.* **2019**, *37*, 266–273. [CrossRef]
13. Zaldivar, R.J.; Witkin, D.B.; Mclouth, T.; Patel, D.N.; Schmitt, K.; Nokes, J.P. Influence of processing and orientation print effects on the mechanical and thermal behavior of 3D-Printed ULTEM 9085 Material. *Addit. Manuf.* **2017**, *13*, 71–80. [CrossRef]
14. Stratasys ULTEM™ 9085 Resin Datasheet. Available online: https://www.stratasys.com/it/materials/search/ultem9085 (accessed on 3 February 2020).
15. Gebisa, A.W.; Lemu, H.G. Investigating Effects of Fused-Deposition Modeling (FDM) Processing Parameters on Flexural Properties of ULTEM 9085 using Designed Experiment. *Materials* **2018**, *11*, 500. [CrossRef]
16. Motaparti, K.P. Effect of build parameters on mechanical properties of ultem 9085 parts by fused deposition modeling. Master's Thesis, Missouri University of Science and Technology, Rolla, MO, USA, 2016. Available online: https://scholarsmine.mst.edu/masters_theses/7513 (accessed on 1 May 2020).
17. Motaparti, K.P.; Taylor, G.; Leu, M.C.; Chandrashekhara, K.; Castle, J.; Matlack, M.; Motaparti, K.P.; Taylor, G.; Leu, M.C.; Chandrashekhara, K. Experimental investigation of effects of build parameters on flexural properties in fused deposition modelling parts. *Virtual Phys. Prototyp.* **2017**, *12*, 207–220. [CrossRef]
18. Chuang, K.C.; Grady, J.E.; Draper, R.D. Additive manufacturing and characterization of Ultem polymers and composites. In Proceedings of the CAMX Conference Proceedings, Dallas, TX, USA, 26–29 October 2015.
19. Bagsik, A.; Schoppner, V. Mechanical Properties of Fused Deposition Modeling Pards with Ultem* 9085. In Proceedings of the 69th Annual Technical Conference of the Society of Plastics Engineers (ANTEC'11), Boston, MA, USA, 1–5 May 2011; pp. 1294–1298.
20. Bagsik, A.; Schoppner, V.; Klemp, E. FDM Part Quality Manufactured with Ultem * 9085. In Proceedings of the 14th International Conference Polymeric Materials 2010, Halle, Germany, 15–17 September 2010; Martin-Luther-University: Halle-Wittenberg, Germany, 2010. ISBN 9783868292824.
21. Roberson, D.A.; Torrado, A.R.; Shemelya, C.M.; Rivera, A.; Macdonald, E.; Wicker, R.B. Comparison of stress concentrator fabrication for 3D printed polymeric izod impact test specimens. *Addit. Manuf.* **2015**, *7*, 1–11. [CrossRef]
22. Cicala, G.; Ognibene, G.; Portuesi, S.; Blanco, I.; Rapisarda, M.; Pergolizzi, E.; Recca, G. Comparison of Ultem 9085 Used in Fused Deposition Modelling (FDM) with Polytherimide Blends. *Materials* **2018**, *11*, 285. [CrossRef] [PubMed]
23. Shelton, T.E.; Willburn, Z.A.; Hartsfield, C.R.; Cobb, G.R.; Cerri, J.T.; Kemnitz, R.A. Effects of thermal process parameters on mechanical interlayer strength for additively manufactured Ultem 9085. *Polym. Test.* **2020**, *81*, 106255. [CrossRef]
24. Bagsik, A.; Schöppner, V.; Klemp, E. Long-term ageing effects on fused deposition modeling parts manufactured with ultem*9085. In Proceedings of the 23rd Annual International Solid Freeform Fabrication Symposium—An Additive Manufacturing Conference, Austin, TX, USA, 22 August 2012; pp. 629–640.
25. Byberg, K.I.; Gebisa, A.W.; Lemu, H.G. Mechanical properties of ULTEM 9085 material processed by fused deposition modeling. *Polym. Test.* **2018**, *72*, 335–347. [CrossRef]

26. Dadour, I.R.; Almanjahie, I.; Fowkes, N.D.; Keady, G.; Vijayan, K. Temperature variations in a parked vehicle. *Forensic Sci. Int.* **2011**, *207*, 205–211. [CrossRef]
27. Guard, A.; Gallagher, S.S. Heat related deaths to young children in parked cars: An analysis of 171 fatalities in the United States, 1995–2002. *Inj. Prev.* **2005**, *11*, 33–37. [CrossRef]
28. Grundstein, A.; Meentemeyer, V.; Dowd, J. Maximum vehicle cabin temperatures under different meteorological conditions. *Int. J. Biometeorol.* **2009**, *53*, 255–261. [CrossRef]
29. Badini, C.; Padovano, E.; Lambertini, V.G. Preferred orientation of chopped fibers in polymer-based composites processed by selective laser sintering and fused deposition modeling: Effects on mechanical properties. *J. Appl. Polym. Sci.* **2020**. [CrossRef]
30. Stratasys FDM Nylon 12CF FDM Nylon 12CF. Available online: https://www.stratasys.com/it/materials/search/fdm-nylon-12cf (accessed on 9 March 2020).
31. Lisa, G.; Hamciuc, C.; Hamciuc, E.; Tudorachi, N. Thermal and thermo-oxidative stability and probable degradation mechanism of some polyetherimides. *J. Anal. Appl. Pyrolysis* **2016**, *118*, 144–154. [CrossRef]
32. Feng, Y.; Wang, B.; Wang, F.; Zhao, Y.; Liu, C.; Chen, J.; Shen, C. Thermal degradation mechanism and kinetics of polycarbonate/silica nanocomposites. *Polym. Degrad. Stab.* **2014**, *107*, 129–138. [CrossRef]

© 2020 by the authors. Licensee MDPI, Basel, Switzerland. This article is an open access article distributed under the terms and conditions of the Creative Commons Attribution (CC BY) license (http://creativecommons.org/licenses/by/4.0/).